Neurobiology of Disease

c-Jun N-Terminal Kinase Promotes Stress Granule Assembly and Neurodegeneration in C9orf72-Mediated ALS and FTD

Talanjeri Gopalakrishna Sahana,[1] Katherine Johnson Chase,[1] Feilin Liu,[1] Thomas E. Lloyd,[2] Wilfried Rossoll,[1,3] and Ke Zhang[1,3,4]

[1]Department of Neuroscience, Mayo Clinic, Jacksonville, Florida 32224, [2]Department of Neurology, Johns Hopkins School of Medicine, Baltimore, Maryland 21205, [3]Neuroscience Graduate Program, Mayo Clinic Graduate School of Biomedical Sciences, Jacksonville, Florida 32224, and [4]Institute of Neurological and Psychiatric Disorders, Shenzhen Bay Laboratory, Gaoke Innovation Centre A16, Guangqiao Rd, Shenzhen, Guangdong 518107, China, P.R.

Stress granules are the RNA/protein condensates assembled in the cells under stress. They play a critical role in the pathogenesis of amyotrophic lateral sclerosis (ALS) and frontotemporal dementia (FTD). However, how stress granule assembly is regulated and related to ALS/FTD pathomechanism is incompletely understood. Mutation in the C9orf72 gene is the most common cause of familial ALS and FTD. C9orf72 mutation causes the formation of toxic dipeptide repeats. Here we show that the two most toxic dipeptide repeats [i.e., poly(GR) and poly(PR)] activate c-Jun N-terminal kinase (JNK) via the ER-stress response protein IRE1 using fly and cellular models. Further, we show that activated JNK promotes stress granule assembly in cells by promoting the transcription of one of the key stress granule proteins (i.e., G3BP1) by inducing histone 3 phosphorylation. Consistent with these findings, JNK or IRE1 inhibition reduced stress granule formation, histone 3 phosphorylation, G3BP1 mRNA and protein levels, and neurotoxicity in cells overexpressing poly(GR) and poly(PR) or neurons derived from male and female C9ALS/FTD patient-induced pluripotent stem cells. Our findings connect ER stress, JNK activation, and stress granule assembly in a unified pathway contributing to C9ALS/FTD neurodegeneration.

Key words: **C9orf72; ER stress; G3BP1; H3S10; JNK; stress granules**

Significance Statement

c-Jun N-terminal kinase (JNK) is a part of the mitogen-activated protein kinase pathway, which is the central node for the integration of multiple stress signals. Cells are under constant stress in neurodegenerative diseases, and how these cells respond to stress signals is a critical factor in determining their survival or death. Previous studies have shown JNK as a major contributor to cellular apoptosis. Here, we show the role of JNK in stress granule assembly. We identify that toxic dipeptide repeats produced in ALS/FTD conditions activate JNK. The activated JNK in the nucleus can induce histone modifications which increase G3BP1 expression, thus promoting stress granule assembly and neurodegeneration.

Introduction

A GGGGCC (G_4C_2) hexanucleotide repeat expansion in chromosome 9, open reading frame 72 (*C9ORF72*) is the most common genetic cause of amyotrophic lateral sclerosis (ALS) and frontotemporal dementia (FTD) (DeJesus-Hernandez et al., 2011; Renton et al., 2011). This repeat expansion can cause cytotoxicity via multiple mechanisms, one of which suggests that it undergoes repeat-associated, non-ATG translation to produce five different species of dipeptide repeat proteins (DPRs), namely, poly(glycine-arginine [GR]), poly(glycine-alanine [GA]), poly(glycine-proline [GP]), poly(proline-alanine [PA]), and poly(proline-arginine [PR]) (Ash et al., 2013; Donnelly et al., 2013; Gendron et al., 2013; Ling et al., 2013; Mori et al., 2013a, 2013b; Zu et al., 2013). Among these DPRs, the arginine-rich DPRs (R-DPRs) i.e., poly(GR), and poly (PR), are especially toxic (Kwon et al., 2014; Mizielinska et al., 2014; K. H. Lee et al., 2016; Lin et al., 2016; Sakae et al., 2018; K. Zhang et al., 2018; Y. J. Zhang et al., 2018, 2019).

Stress granules (SGs) are cytoplasmic RNA/protein condensates assembled in cells under stress (Protter and Parker, 2016). Upon stress, polysomes disassemble, and many RNA-binding

Received Sep. 20, 2022; revised Feb. 9, 2023; accepted Mar. 15, 2023.

Author contributions: T.G.S. and K.Z. designed research; T.G.S. and K.J.C. performed research; T.G.S. and K.Z. analyzed data; T.G.S. and K.Z. wrote the first draft of the paper; T.G.S. edited the paper; T.G.S. wrote the paper; F.L., W.R., and T.E.L. contributed unpublished reagents/analytic tools.

This work was supported by Bloomington Drosophila Stock Center (National Institutes of Health P400D018537, fly stocks). K.Z. was supported by National Institutes of Health, National Institute of Neurological Disorders and Stroke, National Institute on Aging R01NS117461; Department of Defense W81XWH-21-1-0082; Target ALS; and the Frick Foundation for ALS. We thank Yong-Jie Zhang and Karen Jansen-West for the GR_{100}-mCherry constructs.

The authors declare no competing financial interests.

Correspondence should be addressed to Talanjeri Gopalakrishna Sahana at TalanjeriGopalakrishna.Sahana@mayo.edu or Ke Zhang at ke.zhang@szbl.ac.cn.

https://doi.org/10.1523/JNEUROSCI.1799-22.2023

Copyright © 2023 the authors

proteins are recruited to mRNAs, whose condensation mediates SG assembly (Guillen-Boixet et al., 2020; Sanders et al., 2020; Yang et al., 2020). Under normal conditions, SGs are dynamic and disassembled when stress is removed (Lin et al., 2015; Protter and Parker, 2016). However, aberrant SG formation can trigger the aggregation of SG proteins, such as TDP-43 and FUS (Daigle et al., 2013; Coyne et al., 2015). Since the aggregation of these proteins is a pathologic hallmark of ALS and FTD, including C9ALS/FTD, SGs are believed to play a critical role in ALS/FTD pathogenesis (Anderson and Kedersha, 2008; Kedersha et al., 2008; Li et al., 2013). Consistent with this notion, R-DPRs interact with many SG proteins, and their overexpression causes the formation of aberrant, poorly dynamic SGs in cells without additional stress (K. H. Lee et al., 2016; Boeynaems et al., 2017; K. Zhang et al., 2018). In addition, chemically synthesized R-DPRs can undergo liquid-liquid phase separation, recruit SG proteins, and cause SG protein precipitation in cellular lysates (Boeynaems et al., 2017). Also, poly(GR) can localize to SGs, promote the aggregation of recombinant TDP-43 *in vitro*, and co-aggregate with TDP-43 and the SG protein eIF3η in C9ALS/FTD patient postmortem tissue (Cook et al., 2020). In agreement with these data, we previously found that inhibiting SG assembly by genetic or pharmacological approaches suppresses R-DPR-induced cytotoxicity or neurodegeneration in cellular or animal models (K. Zhang et al., 2018). Together, these findings suggest that R-DPRs cause neurodegeneration by promoting aberrant SG formation. However, how this process is regulated is unclear.

In a *Drosophila* RNAi screen, we previously identified that loss of *bsk*, the fly homolog of c-Jun N-terminal kinase (JNK), suppresses neurodegeneration in a fly model of C9ALS/FTD (K. Zhang et al., 2015). Here, we show that JNK is activated in C9ALS/FTD conditions via ER stress response protein IRE1, and activated JNK promotes R-DPR-induced SG formation by promoting the transcription of G3BP1, a key protein involved in SG assembly (Deniz, 2020; Guillen-Boixet et al., 2020; Yang et al., 2020). Inhibiting ER stress responses or JNK activity suppresses R-DPR-induced SG formation, G3BP1 mRNA and protein levels, and cytotoxicity in cells expressing R-DPRs or C9ALS/FTD patient iPSC-derived neurons (iPSNs). Our findings identified a molecular mechanism by which the ER stress/IRE1/JNK axis promotes SG formation and suggested a unified, druggable pathway contributing to C9ALS/FTD pathogenesis.

Materials and Methods

iPSC culture and motor neuron differentiation. Isogenic pairs of iPSCs were previously described (Ababneh et al., 2020), and other iPSC lines from C9orf72 patients (including 2 males and 2 females) and non-neurologic controls (including 2 males and 2 females) were obtained from Cedars-Sinai Stem cell Core (patient demographics are provided in Extended Data Table 5-1). iPSCs were differentiated into direct induced motor neurons (diMNs) using a previously published protocol (Coyne et al., 2020). Briefly, iPSCs were grown in mTeSR media on Matrigel (Corning)-coated 10 cm dishes for 2 weeks before differentiation. At 40% confluency, iPSC colonies were cultured in Stage 1 media containing IMDM 47.5% (Invitrogen), 47.5% F12, 1% NEAA (Invitrogen), 1% Pen/Strep (Invitrogen), 2% B27 (Invitrogen), 1% N2 (Invitrogen), 0.2 μM LDN193189 (Stemgent), 10 μM SB431542 (STEMCELL Technologies), and 3 μM CHIR99021 (Sigma-Aldrich) for 6 d. On day 6, colonies were passaged with accutase (EMD Millipore) and replated on Matrigel-coated 6-well plates. Cells were cultured in Stage 2 media containing IMDM 47.5% (Invitrogen), 47.5% F12, 1% NEAA (Invitrogen), 1% Pen/Strep (Invitrogen), 2% B27 (Invitrogen), 1% N2 (Invitrogen), 0.2 μM LDN193189 (Stemgent), 10 μM SB431542 (STEMCELL Technologies), and 3 μM CHIR99021 (Sigma-Aldrich), 0.1 μM all-trans RA (Sigma-Aldrich), and 1 μM SAG (Cayman Chemicals) until day 12. On day 12, cells were trypsinized (GenClone) and replated on Matrigel-coated 24-well plates for imaging or 6-well plates for biochemistry. Cells were cultured in Stage 3 media containing IMDM 47.5% (Invitrogen), 47.5% F12, 1% NEAA (Invitrogen), 1% Pen/Strep (Invitrogen), 2% B27 (Invitrogen), 1% N2 (Invitrogen), 0.1 μM Compound E (Millipore), 2.5 μM DAPT (Sigma-Aldrich), 0.1 μM db-cAMP (Millipore), 0.5 μM all-trans RA (Sigma-Aldrich), 0.1 μM SAG (Cayman Chemicals), 200 ng/ml ascorbic acid (Sigma-Aldrich), 10 ng/ml BDNF (PeproTech), and 10 ng/ml GDNF (PeproTech) until day 32. All cells were maintained at 37°C and 5% CO_2.

Propidium iodide (PI) staining. Day 32 diMNs were treated with 1 µg/ml of PI (Invitrogen) and one drop of NucBlue (Invitrogen) along with the media and incubated at 37°C and 5% CO_2 for 30 min. Images were acquired using a Zeiss LSM 900 confocal microscope (Carl Zeiss) with an Axiocam 512 color camera and related software. For each condition, 10-15 images were taken.

Drosophila genetics. Drosophila was raised on yeast-cornmeal-molasses food at 25°C. All RNAi fly stocks were procured from Bloomington Drosophila Stock Center.

For eye degeneration assay, *GMR-Gal4, UAS-$(G_4C_2)_{30}$/CyO* were crossed to Canton-S flies or *UAS-RNAi,* and *GMR-Gal4, UAS-$(G_4C_2)_{30}$/+; UAS-RNAi (II or III)* and *GMR-Gal4, UAS-30R/+* were selected and aged at 27°C for 12 d. For R-DPR fly models, *GMR-Gal4, UAS-$(GR)_{36}$/CyO* or *GMR-Gal4, UAS-$(PR)_{36}$/CyO* were crossed to Canton-S flies or *UAS-RNAi,* and *GMR-Gal4, UAS-$(GR/PR)_{36}$/+; UAS-RNAi (II or III)* and *GMR-Gal4, UAS-$(GR/PR)_{36}$/+* were selected for scoring. The external morphology of degenerated eyes was scored using a previously published method (Ritson et al., 2010). Briefly, points were added for necrotic patches, loss of bristles, retinal collapse, loss of ommatidial structure, and depigmentation of the eye. Both the eyes were scored, and the individual scores were combined to give a total "degeneration score" in the range of 0-20. Eye images were captured using a Zeiss SteREO Discovery V8 microscope (Carl Zeiss) with Axiocam 512 color camera and related software.

Cell culture. U-2 OS cells (ATCC, HTB-96) were grown in DMEM (Invitrogen) supplemented with 10% FBS (Invitrogen) and 1% penicillin-streptomycin and maintained at 37°C in a humidified incubator supplemented with 5% CO_2. Transfections were performed using Lipofectamine 3000 (Invitrogen) reagent as per the manufacturer's protocol. At 48 h post-transfection, cells were either fixed and immunostained or lysed for immunoblot. For siRNA knockdown PERK GS9541 (QIAGEN) was used.

Immunofluorescent staining. U-2 OS cells or iPSNs were fixed with 4% PFA for 20 min followed by penetration in 0.2% PBX (PBS with 0.2% Triton X-100) for 20 min at room temperature. For iPSNs, 0.3% PBX was used. Cells were blocked with 3% donkey serum (DS) followed by overnight incubation with primary antibodies in 0.1% TBST (TBS with 0.1% Tween-20) containing 3% DS. Primary antibodies were used as follows: G3BP1 (Abcam, 181149), phospho-H3S10 (Abcam, ab5176, AB_304763) and TIA1 (ProteinTech, 12133-2-AP, AB_2201427), at 1:200 dilutions. Cells were washed 3 times with TBST (20 min each) followed by incubation with secondary antibodies conjugated to AlexaFluor-488, -568, or -647 (1:1000 dilution) in TBST and 3% DS. After that, cells were washed 3 times with TBST (20 min each) and mounted using Prolong antifade Gold mountant (Fisher Scientific).

Images were acquired using Zeiss LSM900 confocal microscope (Carl Zeiss) with an Axiocam 512 color camera and related software.

Plasmid source and construction. The mCherry plasmid was procured from Addgene, and $(GR)_{100}$-mCherry was a gift from Yong-Jie Zhang (Cook et al., 2020). To generate the mCherry-tagged poly-PR expression plasmid, the BioID sequence in myc-BioID-(PR)x100 (F. L. Liu et al., 2022) was replaced with a NdeI/BamHI fragment encoding mCherry followed by a flexible linker (mCherry-GGGSx3).

Drug treatments. U-2 OS cells were treated with JNK inhibitor SP600125 (50 μM) (Selleck Chemicals) for 24 h or with IRE1 inhibitor 4µ8C (50 μM) (Selleck Chemicals) for 6 h and incubated at 37°C.

For iPSNs, day 32 diMNs were stressed with 5 μM of tunicamycin (TM, Sigma-Aldrich) and cotreated with either DMSO or 25-50 μM JNK inhibitor (SP600125) or 25-50 μM IRE1 inhibitor (4µ8C) for 24 h.

Western blot, immunoblot. U-2 OS and iPSNs were lysed in Laemmli buffer and heated to 98°C for 15 min. The protein samples were separated using 4%-15% SDS mini-PROTEAN TGX precast gels (Bio-Rad) and transferred to 0.45 µm nitrocellulose membranes (Bio-Rad). For dot blots, samples were directly blotted on the nitrocellulose membrane and air-dried for 20 min. Blots were blocked with 5% milk for 1 h and incubated overnight with the primary antibody (1:1000 dilution, for actin 1:5000) in 0.1% TBST containing 5% milk. Primary antibodies were used as follows: JNK (Cell Signaling, 9252S, AB_2250373), phospho-JNK (Cell Signaling, 9251S, 162 AB_331659), phospho-H3S10 (Abcam, ab5176, AB_304763), H3 (Cell Signaling, 9715S, AB_331563), IRE1 (Cell Signaling, 3294S, AB_823545), phospho-IRE1 (Abcam, ab48187, AB_873899), TRAF2 (Cell Signaling, 4724S, AB_2209845), phospho-TRAF2 (Cell Signaling, 13908S, AB_2798342), G3BP1 (Abcam, 181149), and TIA1 (ProteinTech, 12 133-2-AP, AB_2201427) at 1:1000 dilutions and actin (EMD Millipore, MAB1501, AB_2223041), mCherry (Abcam, ab167453, AB_2571870) at 1:5000 dilutions. Blots were washed with TBST followed by incubation with HRP-conjugated secondary antibodies in TBST and 5% milk (1:5000 dilution). For mCherry dot blots, BSA was used for blocking instead of milk. Chemiluminescent substrate WesternLigtning Plus-ECL (PerkinElmer) was used for detection. Images were captured using the iBright FL1500 Imaging system (Fisher Scientific).

MTT assay. U-2 OS cells were incubated with media containing MTT (1 mg/ml) at 37°C for 4 h. After that, media was removed and cells were lysed using DMSO, and absorbance was measured at 570 nm using A Tecan Spark multimode microplate reader.

PCR. RNA was isolated from cells using Trizol reagent (Invitrogen) following the manufacturer's protocol. Reverse transcription was done using the SuperScript IV First-Strand Synthesis kit (Invitrogen). qPCR was done using the SYBR-Green Master mix using Applied Biosystem Quant Studio 7. The following primers were used: for *GAPDH* forward 5′-GTTCGACAGTCAGCCGCATC-3′, reverse 5'-GGAATTTGCCATGGGTGGA-3'; for *G3BP1* forward 5′-GTCCTTAGCAACAGGCCCAT-3′, reverse 5′-TTATCTCGTCGGTCGCCTTC-3′. To analyze *XBP1* alternative splicing events, cDNA was amplification using DreamTaq PCR mix (Invitrogen) and separated on 2.5% agarose gel (MetaPhor agarose, Lonza). The following primers were used: *XBP1* forward 5′-TTACGAGAGAAAACTCATGGC-3′, reverse 5′- GGGTCCAAGTTGTCCAGAATGC-3′.

Quantification and statistical analysis. Western blots were quantified using FIJI-just ImageJ. For SG counts and PI staining, at least 300 cells were counted. For p-H3S10 immunostaining, 20-50 cells were counted. The data are presented as mean ± SEM. Statistical analysis was done using paired or unpaired Student's *t* test, one-way ANOVA followed by Dunnett's test/Tukey's test, and χ^2 test as described in the figure legends using GraphPad Prism version 8 (GraphPad).

Results

Loss of *bsk*/JNK suppresses toxicity caused by G_4C_2 repeats and R-DPRs in *Drosophila*

Expression of 30 G_4C_2 repeats [$(G_4C_2)_{30}$] in fly eyes using GMR-GAL4 causes eye degeneration, as indicated by defects in the external eye morphology that worsen with age (Xu et al., 2013; K. Zhang et al., 2015). Using this fly model, our previously published RNAi screen identified *bsk* RNAi to potently suppress $(G_4C_2)_{30}$-mediated eye degeneration (K. Zhang et al., 2015), which we verified here (Fig. 1*A*).

The G_4C_2 repeats translate to produce five DPR species, among which the R-DPRs, i.e., poly(GR) and poly(PR), are highly toxic and cause eye degeneration in *Drosophila* (Mizielinska et al., 2014). We used this model to investigate the *bsk* loss-of-function activity on R-DPR toxicity. *bsk* RNAi suppresses eye degeneration caused by 36 repeats of poly(GR) or poly(PR) (Fig. 1*B*), suggesting that JNK contributes to poly(GR) and poly(PR)-mediated toxicity. Next, to further validate the *bsk* loss-of-function activity, we used U-2 osteosarcoma (OS) cells. These cells are widely used to study R-DPR toxicity and cellular stress responses for their human relevance and ease to dissect cellular mechanisms (Ohn et al., 2008; Kwon et al., 2014; Boeynaems et al., 2017; Yang et al., 2020). We expressed mCherry-tagged, 100 repeats of poly(GR) or poly(PR) [$(GR)_{100}$- or $(PR)_{100}$-mCherry] for 48 h in U-2 OS cells, and mCherry alone was used as a control. Western blots of cell lysates and immunofluorescent staining of poly(GR) and poly(PR) expressing cells show an increase in the levels of phosphorylated JNK (pJNK), the activated JNK form, compared with the mCherry control (Fig. 1*C*,*D*). Next, using an MTT cell survival assay, we show that 24 h cotreatment of a pan-JNK inhibitor (SP600125) post-transfection suppressed poly(GR) and poly(PR) induced cytotoxicity and increased cell survival as measured by MTT levels in U-2 OS cells (Fig. 1*E*). The fly and cell culture data consistently suggest that JNK/*bsk* is activated by G_4C_2 repeats through R-DPR expression and the loss of *bsk*/JNK reduces their cytotoxicity.

JNK/*bsk* is activated by ER stress via IRE1 and inhibition of IRE1 reduces G_4C_2 and R-DPR toxicity

bsk/JNK belongs to the mitogen-activated protein kinase (MAPK) family, which is activated in response to several intracellular or extracellular stress signals, including ER stress (Urano et al., 2000; Nishitoh et al., 2002; Kim and Choi, 2010; Sahana and Zhang, 2021). Several studies have shown the accumulation of misfolded proteins in the ER and the activation of unfolded protein response (UPR) pathways in multiple ALS models (Kikuchi et al., 2006; Nishitoh et al., 2008; Y. J. Zhang et al., 2014; Dafinca et al., 2016; S. Lee et al., 2016; Cheng et al., 2018; Medinas et al., 2018; Thams et al., 2019). In addition, the selective vulnerability of motor neurons (MNs) in ALS conditions is still not understood and chronic ER stress could be a potential risk factor for MN death (Haeusler et al., 2014; Dafinca et al., 2016). So, to evaluate whether ER stress activates JNK in C9 conditions, in $(G_4C_2)_{30}$ fly models, we knocked down UPR genes. Knockdown of PERK, and IRE1 but not ATF6 rescued eye degeneration caused by $(G_4C_2)_{30}$ repeats (Extended Data Fig. 2-1*A*). Further, in U-2 OS cells expressing poly(GR) and poly(PR), we inhibited PERK and IRE1. Inhibition of IRE1 reduced JNK activation as measured by pJNK levels (Fig. 2*A*) but not by PERK (Extended Data Fig. 2-1*B*). This suggests that R-DPR-induced UPR activates JNK via IRE1 activation in C9orf72-mediated ALS/FTD.

IRE1 is a UPR protein that is dimerized and activated in response to misfolded protein stress in the ER (Walter and Ron, 2011). Activated IRE1 has a kinase domain responsible for signal transduction through kinase activity and an endonuclease domain involved in unconventional splicing of the transcription factor XBP1, which further can induce UPR inducible genes including chaperones (Adams et al., 2019). Of note, 4µ8C, a pharmacological inhibitor of IRE1, inhibits both IRE1 kinase and endonuclease activities (Cross et al., 2012), and the reduction of pJNK levels by inhibition of IRE1 using 4µ8C suggests that IRE1 is activated in C9orf72-mediated ALS/FTD conditions. To verify this, we collected cell lysates from U-2 OS cells expressing poly(GR) and poly(PR). Lysates showed increased p-IRE1, p-TRAF2 levels (an adapter protein that binds to activated IRE1 and is involved in signal transduction), and an alternative splice variant of XBP1 in poly(GR) and poly(PR) expressing cells compared with control (Fig. 2*B*; Extended Data Fig. 2-1*C*).

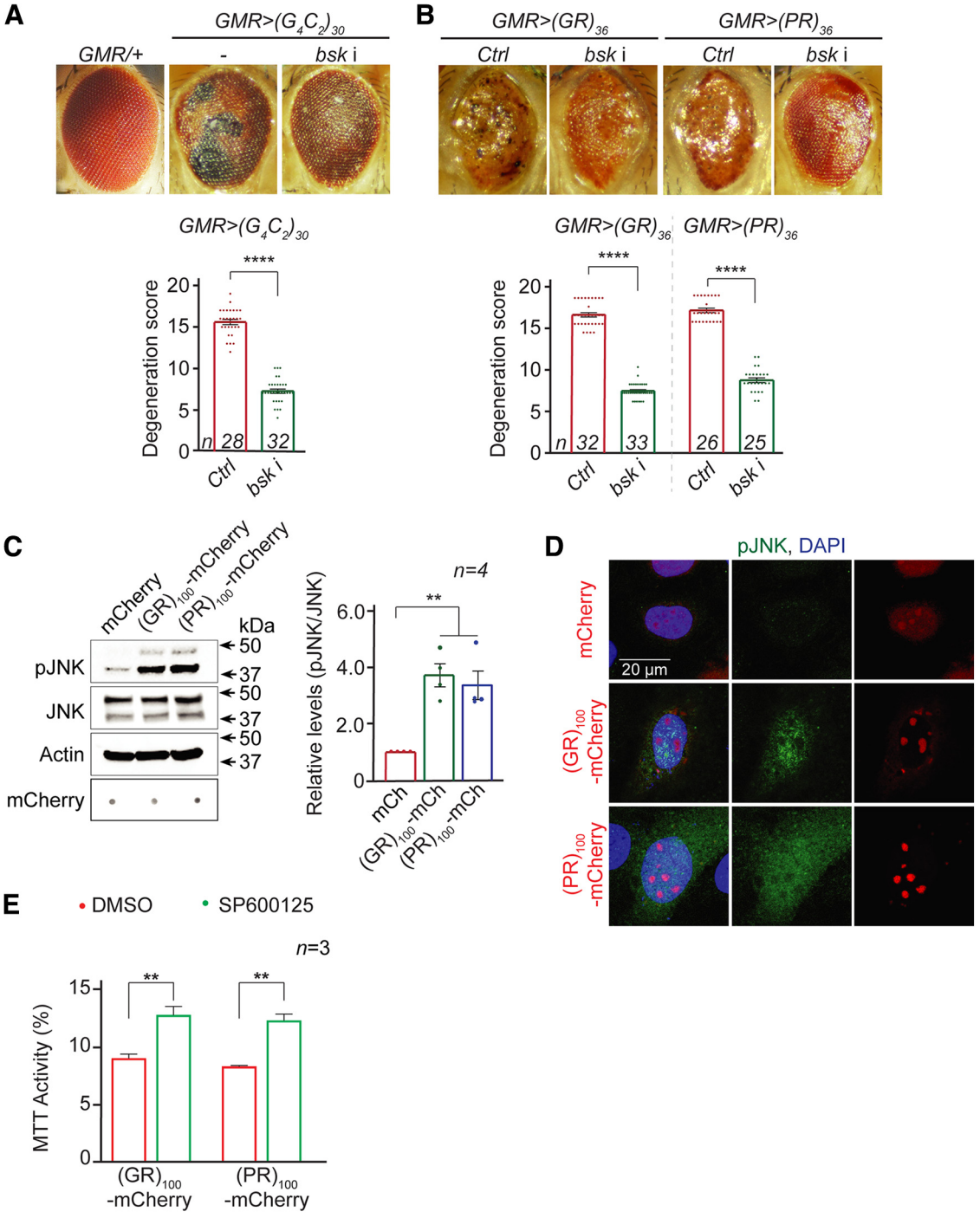

Figure 1. JNK/*bsk* is activated in a fly and cellular model of C9ALS/FTD. Fly eyes expressing (***A***) $(G_4C_2)_{30}$ and (***B***) $(GR)_{36}$ or $(PR)_{36}$ using GMR-GAL4, without or with *bsk* RNAi (*bsk* i). Scored using a previously published method (Ritson et al., 2010). Data are mean ± SEM. ****$p < 0.0001$ (Student's *t* test). ***C***, Western or dot (for mCherry only) blots of lysates from U-2 OS cell expressing mCherry or $(GR/PR)_{100}$-mCherry probed for JNK, pJNK, actin, and mCherry. Data are mean ± SEM. **$p < 0.01$ (one-way ANOVA followed by Dunnett's test). ***D***, U-2 OS cells expressing mCherry or $(GR/PR)_{100}$-mCherry (red) stained with pJNK (green) and DAPI (blue). ***E***, MTT assays of U-2 OS cells expressing mCherry or $(GR/PR)_{100}$-mCherry, treated with DMSO or 50 μM of SP600125 for 24 h. MTT activity of U-2 OS cells expressing mCherry alone is considered as 100% activity. Data are mean ± SEM. **$p < 0.01$ (Student's *t* tests).

Further, we analyzed whether inhibition of either IRE1 or TRAF2 could rescue C9orf72 toxicity. In flies expressing 30 repeats of G_4C_2 and 36 repeats of poly(GR) and poly(PR), knockdown of fly *Ire1* and *Traf2* rescued eye degeneration phenotype (Fig. 2*C*). These results show that DPRs induce ER stress that activates IRE1 which can further activate JNK and the inhibition of ER stress response gene IRE1 or TRAF2 could rescue C9orf72 mediated toxicity.

Inhibition of JNK or IRE1 activity suppresses R-DPR-induced SG formation in U-2 OS cells

Previous studies have shown that ER stress induces protein aggregation in patient tissues and SOD1 transgenic mouse models (Medinas et al., 2018). SGs are believed to be the crucible of protein aggregation (Li et al., 2013) and indeed R-DPRs can induce poorly dynamic SGs in cultured cells without additional stress (K. H. Lee et al., 2016; Boeynaems et al., 2017). When expressed in U-2 OS cells for 48 h,

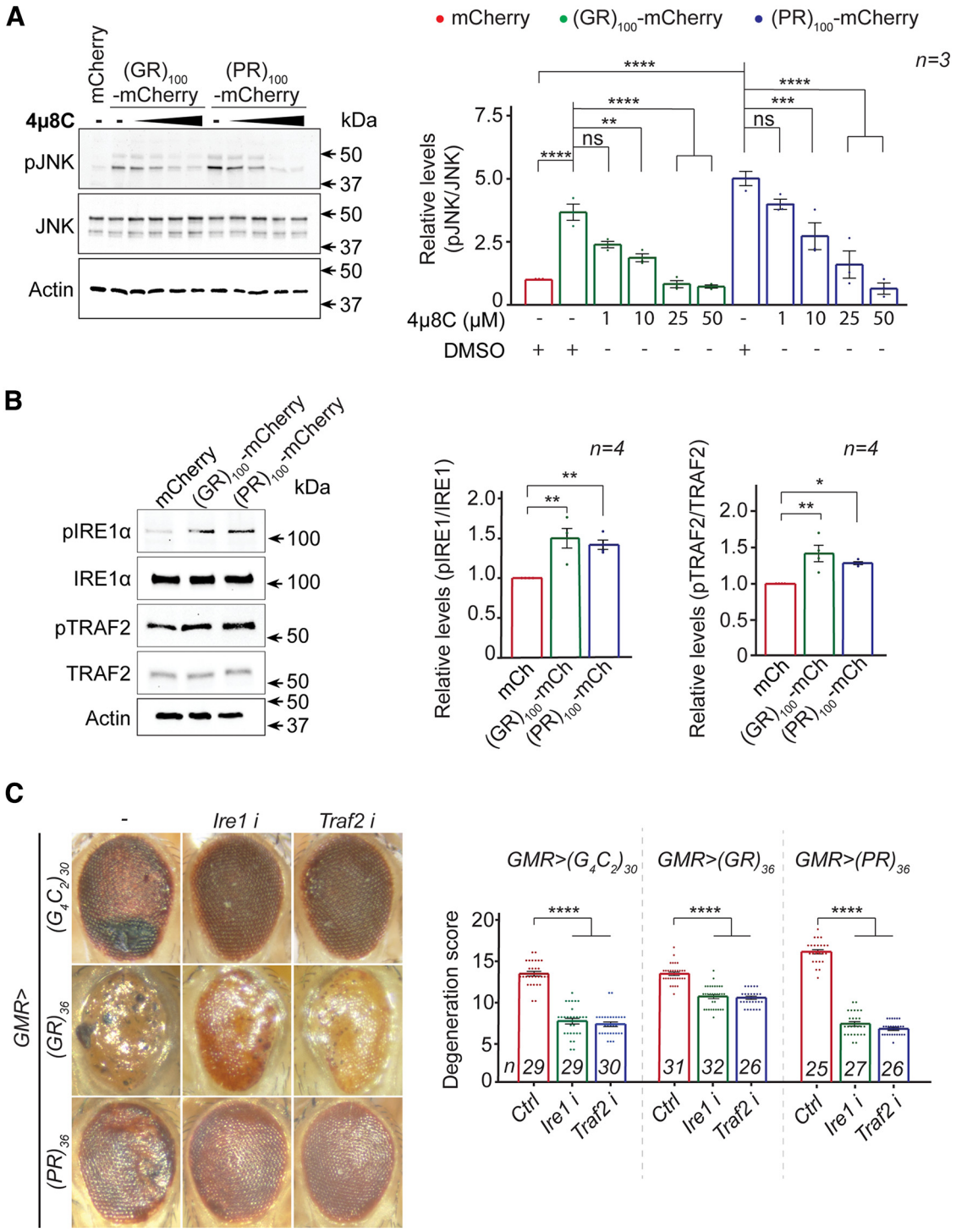

Figure 2. R-DPR-induced ER stress activates JNK via IRE1 in C9ALS/FTD. ***A***, Western blots of lysates from U-2 OS cell expressing mCherry or $(GR/PR)_{100}$-mCherry cotreated with DMSO or 4μ8C for 6 h probed for JNK, pJNK, and actin. Data are mean ± SEM. $^{****}p < 0.0001$; $^{***}p < 0.001$; $^{**}p < 0.01$; one-way ANOVA followed by Tukey's test. ***B***, Western or dot (for mCherry only) blots of lysates from U-2 OS cell expressing mCherry or $(GR/PR)_{100}$-mCherry TRAF2, pTRAF2, IRE1, pIRE1, and actin. Data are mean ± SEM. $^{**}p < 0.01$; $^{*}p < 0.05$; one-way ANOVA followed by Dunnett's test. ***C***, Fly eyes expressing $(G_4C_2)_{30}$ or $(GR)_{36}/(PR)_{36}$ using GMR-GAL4, without or with *Ire1, Traf2* RNAi. Data are mean ± SEM. $^{****}p < 0.0001$ (Student's *t* test). Data showing that IRE1, but not PERK and ATF6, is upstream of pJNK are provided in Extended Data Figure 2-1.

poly(GR) and poly(PR), respectively, causes ~70% or ~30% of cells to exhibit cytoplasmic granules that are positively stained by both G3BP1 and TIA1, two SG markers, suggesting that they are SGs (Fig. 3; Extended Data Fig. 3-1). Furthermore, treating the cells with JNK inhibitor SP600125 (50 μM) for 24 h or IRE1 inhibitor 4μ8C (50 μM) for 6 h post-transfection significantly decreases the percent of cells exhibiting SGs, but not R-DPR protein levels (Fig. 3; Extended Data Fig. 3-1), suggesting that IRE1/JNK promotes R-DPR-induced SG assembly. Different time points for drug treatment were selected based on the optimization (data not shown).

JNK promotes the expression of G3BP1 in U-2 OS cells

G3BP1 plays a critical role in SG assembly, as its knockdown strongly reduces SG formation caused by a variety of stressors,

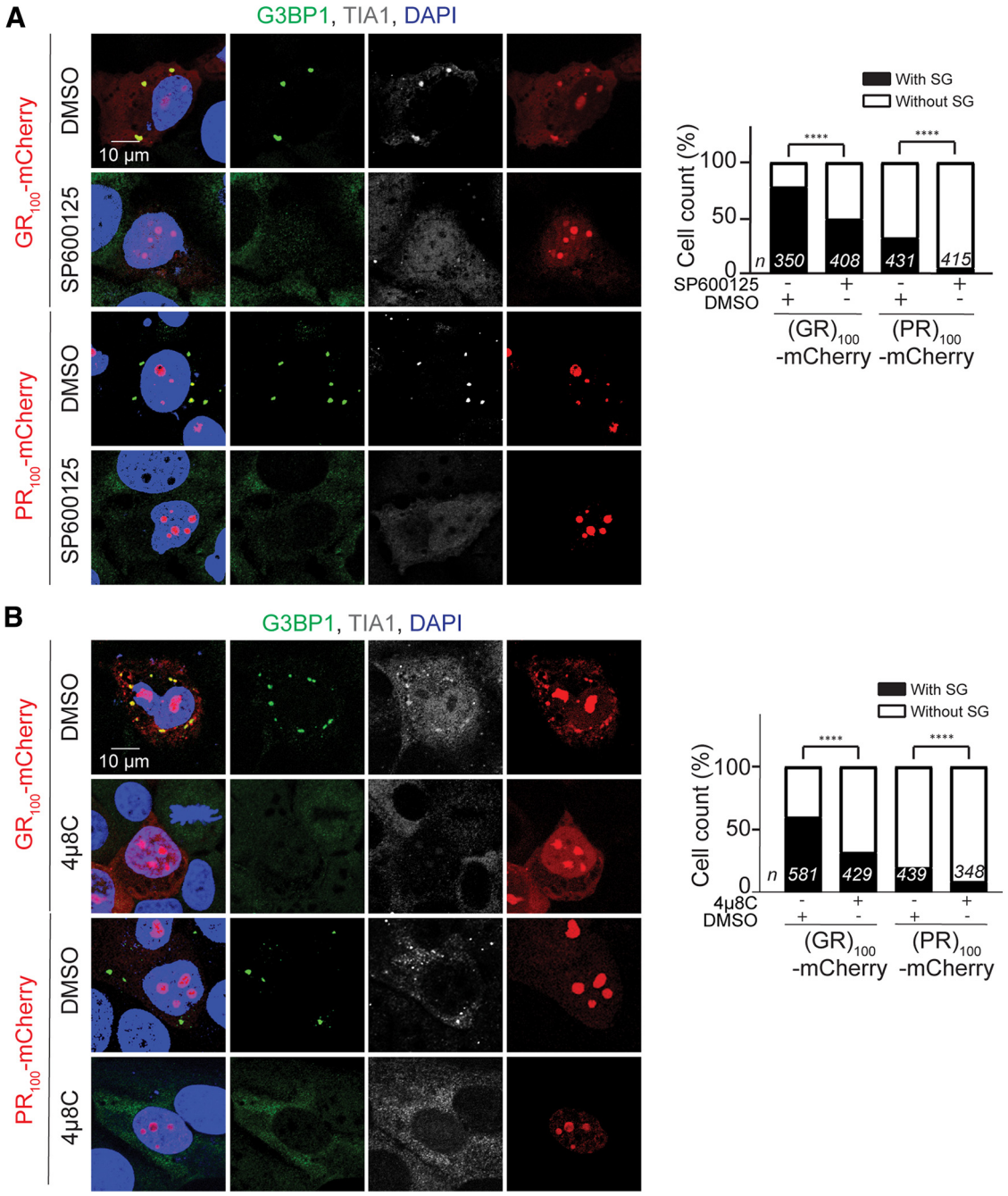

Figure 3. JNK and IRE1 activity promotes R-DPR-induced SG assembly in U-2 OS cells. U-2 OS cells expressing $(GR/PR)_{100}$-mCherry (red) treated with DMSO, (***A***) 50 μM SP600125, or (***B***) 50 μM 4μ8C and stained with G3BP1 (green), TIA1 (white), and DAPI (blue). Quantification showing the percent of cells with or without SGs. ****$p < 0.0001$ (χ^2 test). Large views of the microscopic field are provided in Extended Data Figure 3-1.

whereas its overexpression induces SG formation without additional stress (Kedersha et al., 2016). In addition, we and others found that double KO of G3BP1 and its homolog, G3BP2, completely abolishes R-DPR-induced SGs (Boeynaems et al., 2017; K. Zhang et al., 2018). Here, we show that the treatment of SP600125 or 4μ8C strongly decreases G3BP1 protein levels in cells expressing poly(GR) and poly(PR) (Fig. 4*A*), suggesting that JNK inhibition downregulates G3BP1. In addition, we found that these inhibitors do not reduce TIA1 levels (Extended Data Fig. 4-1*A*), suggesting that JNK regulates specific SG proteins.

A U-2 OS cell line stably expressing GFP-tagged G3BP1 (G3BP1-GFP) under the control of a lentiviral promoter is widely used to study SG biology (Figley et al., 2014). We found that SP600125 suppresses the level of endogenous G3BP1, but not G3BP1-GFP, in these cells when transfected with poly(GR) and poly(PR) (Extended Data Fig. 4-1*B*), possibly because the regulation of JNK on G3BP1 relies on the genomic promoter of *G3BP1*. If this is the case, JNK inhibition likely suppresses *G3BP1* transcription. Indeed, as shown in Figure 4*C*, SP600125 significantly decreases *G3BP1* mRNA levels in poly(GR) and poly(PR) expressing cells compared with untreated cells suggesting that JNK regulates G3BP1 at the transcriptional level in these cells.

A prior study in mouse differentiating neurons showed that activated JNKs in the nucleus are enriched in the promoter regions of certain genes, including G3BP1, where they phosphorylate certain chromatin components i.e., histone 3 protein at

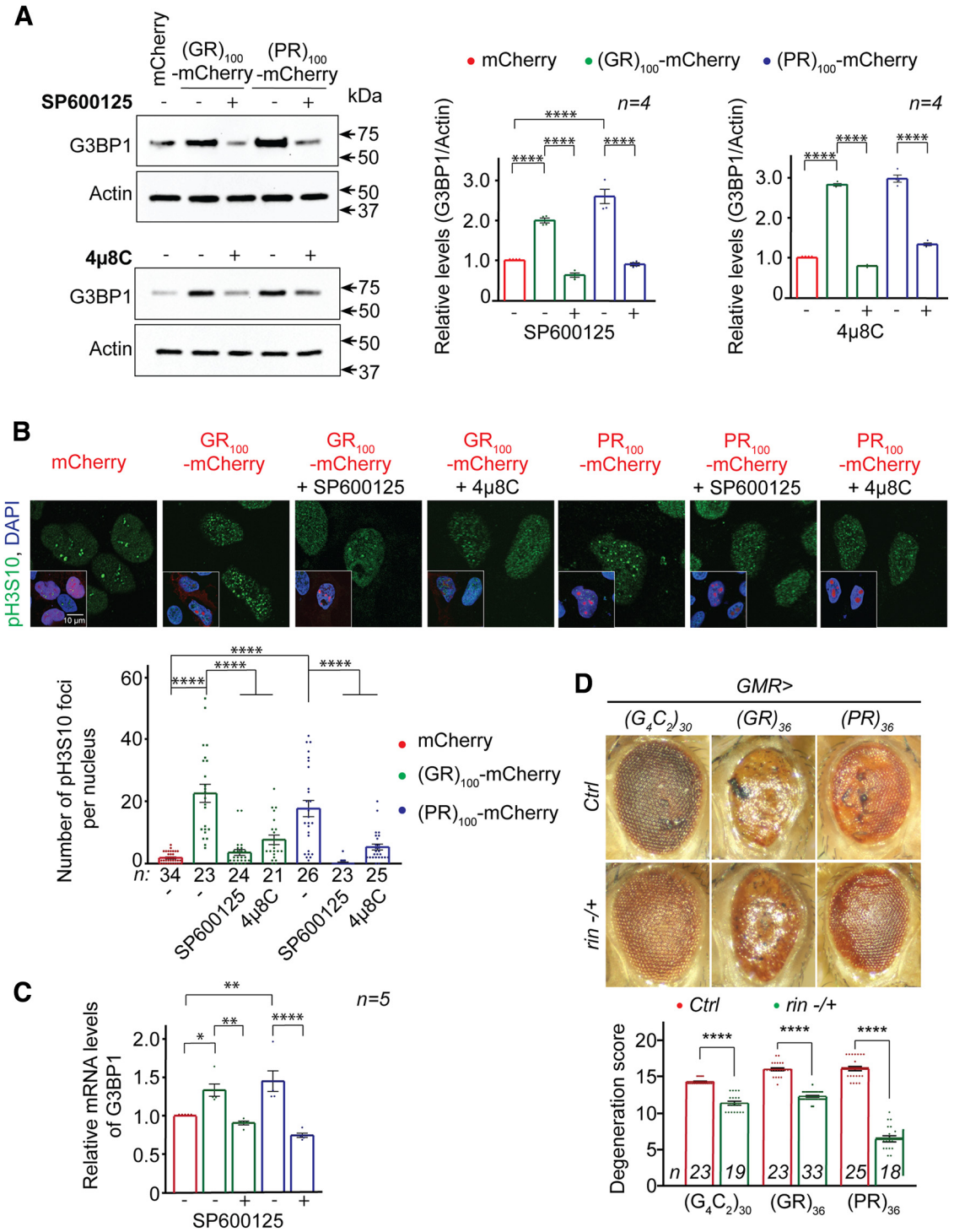

Figure 4. JNK promotes H3S10 phosphorylation and G3BP1 expression in U-2 OS cells expressing R-DPRs. ***A***, Western blots of lysates from U-2 OS cells expressing $(GR/PR)_{100}$-mCherry, treated with DMSO or (***A***) 50 μM SP600125 and (***B***) 50 μM 4μ8C probed for G3BP1. ****$p < 0.0001$ (one-way ANOVA followed by Tukey's test). ***B***, U-2 OS cells expressing $(GR/PR)_{100}$-mCherry (red) treated with DMSO, 50 μM SP600125, or 50 μM 4μ8C and stained with p-H3S10 (green), and DAPI (blue). Quantification showing the number of p-H3S10 foci per nucleus. ****$p < 0.0001$ (one-way ANOVA followed by Dunnett's test). ***C***, Relative levels of G3BP1 mRNA compared with GAPDH from U-2 OS cells expressing $(GR/PR)_{100}$-mCherry, treated with DMSO or 50 μM SP600125. Data are mean ± SEM. ****$p < 0.0001$; **$p < 0.01$; *$p < 0.05$; Student's *t* tests. ***D***, Fly eyes expressing $(G_4C_2)_{30}$, $(GR)_{36}$, or $(PR)_{36}$, without (Ctrl) or with heterozygous loss of function of rin. Data are mean ± SEM. ****$p < 0.0001$ (Student's *t* tests). Data showing no change in TIA1 and lentiviral promoter controlled G3BP1 levels in response to JNK/IRE1 inhibition are provided in Extended Data Figure 4-1.

Serine10 position (H3S10) (Tiwari et al., 2011). As H3S10 phosphorylation (pH3S10) causes the chromatin to adopt an "open" chromatin structure, which activates transcription (Rossetto et al., 2012; Allis and Jenuwein, 2016; Stricker et al., 2017), one possible mechanism by which JNK regulates *G3BP1* transcription is via pH3S10. However, our Western blot analyses did not show any global increase in pH3S10 level in U-2 OS cells transfected with poly(GR) or poly(PR), compared with the mCherry control (Extended Data Fig. 4-1C). To better understand how poly(GR) and poly(PR) affect pH3S10 at the single-cell level, we performed

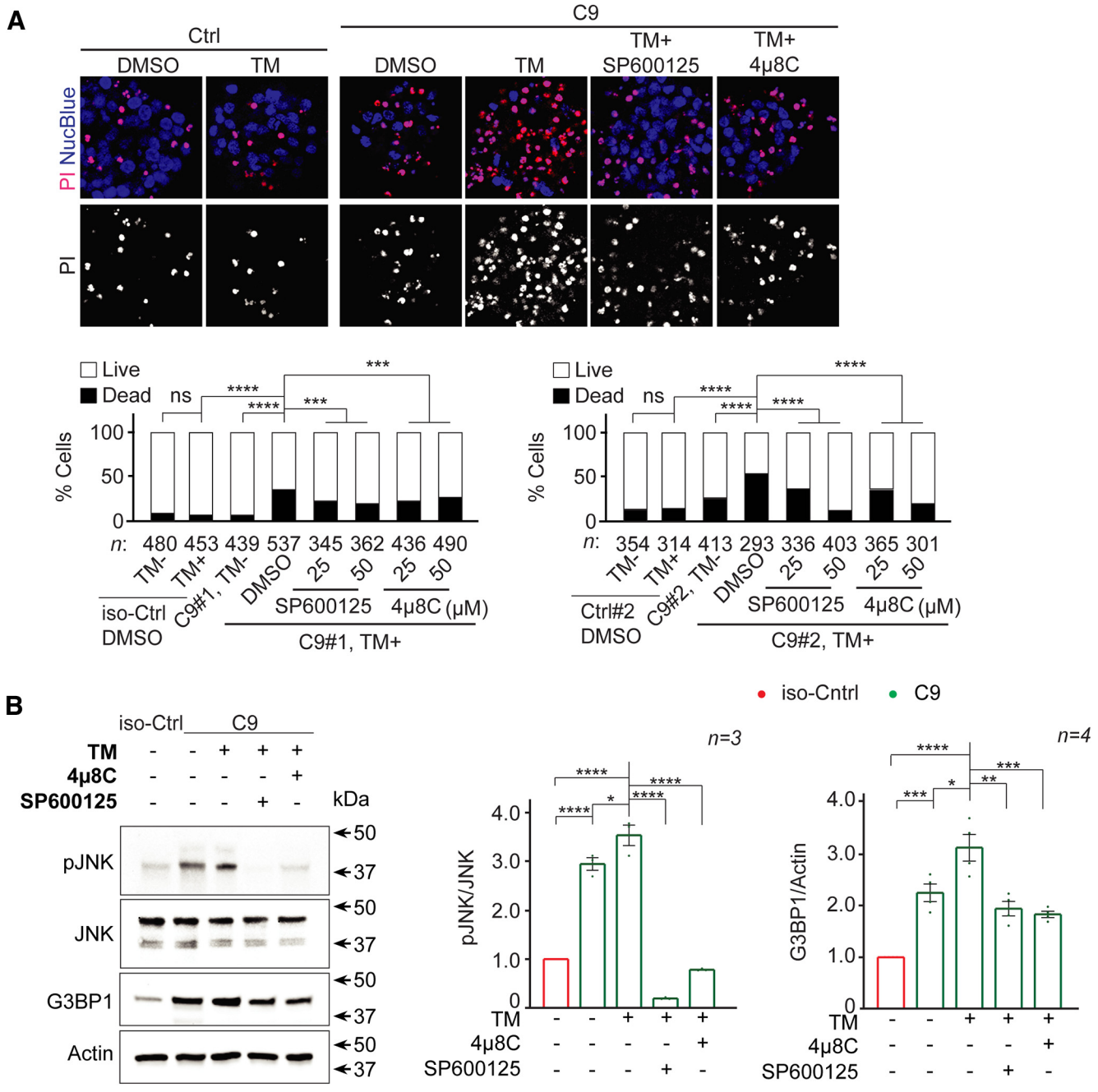

Figure 5. Inhibition of JNK or IRE1 suppresses toxicity in iPSC-derived motor neurons. ***A***, Representative image of control (Ctrl) and C9ALS/FTD (C9) iPSC derived MNs stressed with 5 μM TM followed by treatment with DMSO, SP600125, or 4μ8C and stained with PI (dead cells) and NucBlue (all cells). Quantification shows the percent of live and dead cells in two cell lines, including an isogenic pair. Data are mean ± SEM. ****$p < 0.0001$ (χ^2 test). ***B***, Western blot of C9 lysates treated with 5 μM TM together with DMSO, JNK inhibitor SP600125, or IRE1 inhibitor 4μ8C probed for JNK, pJNK, G3BP1, and actin. Isogenic control is included. Data are mean ± SEM. ****$p < 0.0001$; ***$p < 0.001$; **$p < 0.01$; *$p < 0.05$; one-way ANOVA followed by Tukey's test. Patient demographics of the donors are provided in Extended Data Table 5-1. Quantification of percent of live and dead cells in additional three cell lines is provided in Extended Data Figure 5-2.

immunofluorescent staining of transfected cells and found that pH3S10 levels are readily elevated in cells expressing poly(GR) or poly(PR), compared with the mCherry control (Fig. 4*B*). Interestingly, we found that pH3S10 foci increases in the nucleus of cells expressing poly(GR) or poly(PR), consistent with the notion that JNKs are enriched at only certain regions of the chromosome. Moreover, SP600125 or 4μ8C decreases pH3S10 levels (Fig. 4*B*; Extended Data Fig. 4-1*C*). Together, our data suggest that poly(GR) and poly(PR) increase pH3S10, which is suppressed by JNK or IRE1 inhibition.

Loss of G3BP/Rin suppresses neurodegeneration in C9ALS/FTD fly models

Previously, we showed that G3BP1/2 double KO abolishes R-DPR-induced cellular defects in U-2 OS cells and SG inhibitors GSK2606414 and ISRIB suppress $(G_4C_2)_{30}$-mediated eye degeneration in flies (K. Zhang et al., 2018), suggesting that inhibiting SG formation suppresses C9ALS/FTD-related cytotoxicity or neurodegeneration. Given the importance of G3BP in SG assembly, we postulate that loss of G3BP also suppresses neurodegeneration. In flies, *rin* is the homolog of mammalian *G3BP*. Here,

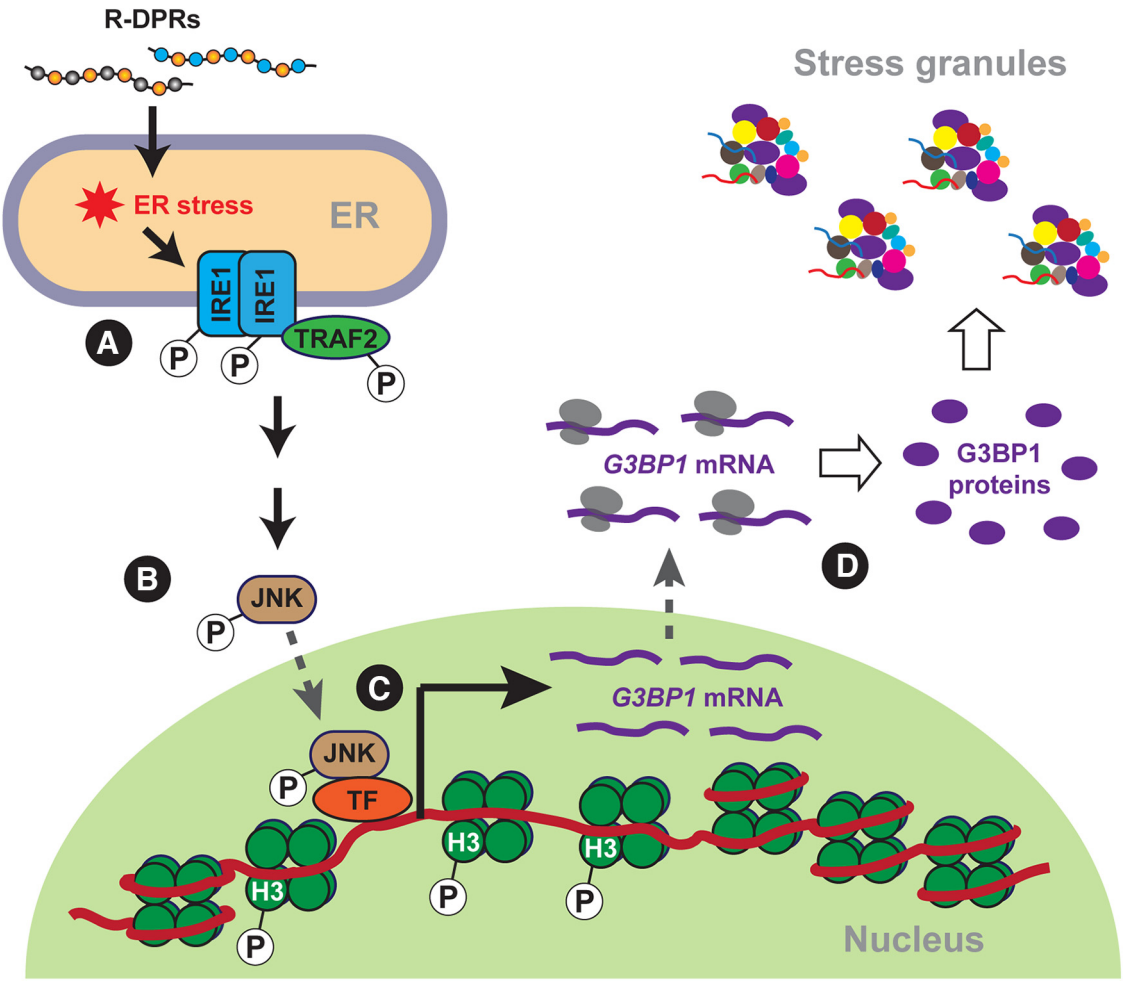

Figure 6. Schematic representation of ER stress/JNK promoting SG assembly in C9ALS/FTD. ***A***, R-DPRs induce ER stress, activating IRE1 and TRAF2. ***B***, Activated IRE1/TRAF2 complex activates JNK. Activated JNK translocates to the nucleus and localizes to the promoter region of *G3BP1*, where it phosphorylates H3 at Serine10. ***C***, H3S10 phosphorylation relaxes DNA, allowing the expression of *G3BP1*. ***D***, The G3BP1 protein level is upregulated, causing SG assembly.

we show that a loss-of-function *rin* mutation heterozygously suppresses eye degeneration caused by $(G_4C_2)_{30}$, $(GR)_{36}$, or $(PR)_{36}$ (Fig. 4*D*), suggesting that loss of G3BP/Rin suppresses neurodegeneration in fly models of C9orf72-mediated ALS/FTD.

Inhibition of IRE1/JNK activity suppresses neurotoxicity in iPSC-derived motor neurons (MNs)

To validate the findings obtained from fly and U-2 OS cells in neuronal cultures, we used iPSCs derived from C9orf72 ALS/FTD patient tissues. We have previously shown that SG inhibitors GSK2606414 and ISRIB, which suppress R-DPR-induced SG formation, suppress subcellular defects in these iPSNs, suggesting that SG assembly contributes to the iPSN toxicity (K. Zhang et al., 2018). While these C9ALS/FTD iPSNs rarely exhibit SGs under nonstressed conditions, they are still constitutively under a low level of stress, as indicated by a mild increase in the phospho-eIF2α (K. Zhang et al., 2018).

Here, we differentiated five pairs of control and C9orf72 iPSCs, including an isogenic pair into MNs. We obtained ~95% MAP2-positive (neuronal marker) and 27.48 ± 5.56% and 36.86 ± 1.30% of Islet-1-positive cells (motor neuron marker), in control and C9orf72 iPSCs, respectively, which is similar to a previous publication (Coyne et al., 2020) (Extended Data Fig. 5-2*A*). The C9 iPSNs showed a slight increase in p-JNK levels compared with the control under nonstressed conditions (Extended Data Fig. 5-2*C*). We further used an ER stressor TM to elicit ER stress in these cells, which is consistent with other studies (Donnelly et al., 2013; Haeusler et al., 2014; Shi et al., 2018). We show that a 24 h treatment of TM (5 μM) increases cell death, as indicated by PI staining, in five pairs of C9ALS/FTD iPSN lines tested, which is suppressed by cotreatments of either JNK inhibitor SP600125 or IRE1 inhibitor 4μ8C (Fig. 5*A*; Extended Data Fig. 5-2*B*). Further, we collected cell lysates from isogenic and C9 iPSNs to evaluate the protein levels. In agreement with the above data, we observed that in C9 iPSCNs, TM treatment increased pJNK levels, which can further be suppressed by either inhibition of JNK or IRE1 activity (Fig. 5*B*). Likewise, G3BP1 levels were increased on TM treatment, which could be significantly reduced by JNK/IRE1 inhibition (Fig. 5*B*), thus validating the results obtained in U-2 OS cell and fly models. Together, these data suggest that inhibiting IRE1/JNK activity suppresses the G3BP1 level and neurotoxicity in C9orf72 ALS/FTD iPSNs.

Discussion

Previous studies identified critical roles of the MAPK/JNK pathway in stress responses and neurodegeneration, including ALS. JNK induces apoptosis in a mouse model of SOD1-mediated ALS (S. Lee et al., 2016) causes energy deficiencies in a mouse

model of Wallerian degeneration (Yang et al., 2015), and disrupts lipid metabolism because of mitochondrial oxidative stress in fly and mouse models (L. Liu et al., 2015). Our finding that JNK promotes SG formation in cellular models of C9ALS/FTD identifies a novel route by which this pathway contributes to stress responses and neurodegeneration, suggesting a broader role of MAPK/JNK.

Despite the importance of SGs in ALS/FTD pathogenesis, it is unclear how SG assembly is regulated at the cellular level and whether this regulation is related to pathomechanism. Here, we show that the ER stress/IRE1/JNK axis promotes SG formation caused by R-DPRs and contributes to neurodegeneration in fly and cellular models of C9ALS/FTD. Mechanistically, activated JNK promotes the *G3BP1* transcription, likely by phosphorylating H3S10, thereby increasing the G3BP1 protein level (Fig. 6). Together, our findings suggest a novel pathway regulating SG formation, which contributes to ALS/FTD pathogenesis.

How JNK promotes G3BP1 transcription is unclear. A previous study showed that in mice neurons, the transcription factor complex nuclear factor Y (NF-Y) and active JNK are recruited to promoter regions of some genes, including *G3BP1* (Tiwari et al., 2011), where activated JNK phosphorylates H3S10, thereby allowing NF-Y-mediated *G3BP1* transactivation. Future studies can test this model in U-2 OS and iPSN models of C9ALS/FTD.

In addition to G3BP1, many other proteins are critical to SG assembly. Thus, future studies can include a comprehensive analysis of proteins that are affected by JNK. Another limitation of this study is that C9ALS/FTD iPSNs do not readily form SGs under nonstressed conditions. Several stressors, such as sodium arsenite, etc., have been used in the literature to stress iPSNs (Donnelly et al., 2013; Haeusler et al., 2014; Shi et al., 2018; K. Zhang et al., 2018). These stressors induce stress in a short period (~1 h) and prolonged stress causes neuronal death; hence, they are not ideal to study the aforementioned JNK activity. However, in our earlier study, we have shown that phospho-eIF2α is increased in these iPSNs, compared with the control, suggesting that these neurons are constantly under low levels of stress (K. Zhang et al., 2018).

Although SP600125 and 4μ8C suppress DPR-induced U-2 OS cell death, the effect is mild, suggesting that either an additional mechanism contributes to the cell death phenotype or these drugs have deleterious effects. In addition to the MAPK/JNK pathway, other pathways and processes are also known to contribute to SG formation, and targeting some of these pathways/processes suppresses neurodegeneration or cytotoxicity in ALS/FTD models (Gilks et al., 2004; Kedersha et al., 2008; Ohn et al., 2008; Jain et al., 2016; Kedersha et al., 2016; Becker et al., 2017; K. Zhang et al., 2018). However, the complex network regulating SG formation in cells is far from understood. Mass spectrometry analyses identified ~400 proteins in yeast and mammalian SGs (Jain et al., 2016), and genetic screens identified >300 genes whose loss limits or reduces arsenite-induced SG formation in U-2 OS cells (Ohn et al., 2008; Yang et al., 2020). For most of these proteins/genes, how they contribute to SG formation and whether they are implicated in ALS/FTD pathogenesis are unclear. Future studies addressing these questions will provide a better understanding of SG biology and potentially identify novel therapeutic targets for the diseases.

References

Ababneh NA, Scaber J, Flynn R, Douglas A, Barbagallo P, Candalija A, Turner MR, Sims D, Dafinca R, Cowley SA, Talbot K (2020) Correction of amyotrophic lateral sclerosis-related phenotypes in induced pluripotent stem cell-derived motor neurons carrying a hexanucleotide expansion mutation in C9orf72 by CRISPR/Cas9 genome editing using homology-directed repair. Hum Mol Genet 29:2200–2217.

Adams CJ, Kopp MC, Larburu N, Nowak PR, Ali MM (2019) Structure and molecular mechanism of ER stress signaling by the unfolded protein response signal activator IRE1. Front Mol Biosci 6:11.

Allis CD, Jenuwein T (2016) The molecular hallmarks of epigenetic control. Nat Rev Genet 17:487–500.

Anderson P, Kedersha N (2008) Stress granules: the Tao of RNA triage. Trends Biochem Sci 33:141–150.

Ash PE, Bieniek KF, Gendron TF, Caulfield T, Lin WL, DeJesus-Hernandez M, Van Blitterswijk MM, Jansen-West K, Paul JW III, Rademakers R, Boylan KB, Dickson DW, Petrucelli L (2013) Unconventional translation of C9ORF72 GGGGCC expansion generates insoluble polypeptides specific to c9FTD/ALS. Neuron 77:639–646.

Becker LA, Huang B, Bieri G, Ma R, Knowles DA, Jafar-Nejad P, Messing J, Kim HJ, Soriano A, Auburger G, Pulst SM, Taylor JP, Rigo F, Gitler AD (2017) Therapeutic reduction of ataxin-2 extends lifespan and reduces pathology in TDP-43 mice. Nature 544:367–371.

Boeynaems S, et al. (2017) Phase separation of C9orf72 dipeptide repeats perturbs stress granule dynamics. Mol Cell 65:1044–1055.e5.

Cheng W, Wang S, Mestre AA, Fu C, Makarem A, Xian F, Hayes LR, Lopez-Gonzalez R, Drenner K, Jiang J, Cleveland DW, Sun S (2018) C9ORF72 GGGGCC repeat-associated non-AUG translation is upregulated by stress through eIF2alpha phosphorylation. Nat Commun 9:51.

Cook CN, et al. (2020) *C9orf72* poly(GR) aggregation induces TDP-43 proteinopathy. Sci Transl Med 12:eabb3774.

Coyne AN, Yamada SB, Siddegowda BB, Estes PS, Zaepfel BL, Johannesmeyer JS, Lockwood DB, Pham LT, Hart MP, Cassel JA, Freibaum B, Boehringer AV, Taylor JP, Reitz AB, Gitler AD, Zarnescu DC (2015) Fragile X protein mitigates TDP-43 toxicity by remodeling RNA granules and restoring translation. Hum Mol Genet 24:6886–6898.

Coyne AN, Zaepfel BL, Hayes L, Fitchman B, Salzberg Y, Luo EC, Bowen K, Trost H, Aigner S, Rigo F, Yeo GW, Harel A, Svendsen CN, Sareen D, Rothstein JD (2020) G4C2 repeat RNA initiates a POM121-mediated reduction in specific nucleoporins in C9orf72 ALS/FTD. Neuron 107:1124–1140.e11.

Cross BC, Bond PJ, Sadowski PG, Jha BK, Zak J, Goodman JM, Silverman RH, Neubert TA, Baxendale IR, Ron D, Harding HP (2012) The molecular basis for selective inhibition of unconventional mRNA splicing by an IRE1-binding small molecule. Proc Natl Acad Sci USA 109:E869–E878.

Dafinca R, Scaber J, Ababneh N, Lalic T, Weir G, Christian H, Vowles J, Douglas AG, Fletcher-Jones A, Browne C, Nakanishi M, Turner MR, Wade-Martins R, Cowley SA, Talbot K (2016) C9orf72 hexanucleotide expansions are associated with altered endoplasmic reticulum calcium homeostasis and stress granule formation in induced pluripotent stem cell-derived neurons from patients with amyotrophic lateral sclerosis and frontotemporal dementia. Stem Cells 34:2063–2078.

Daigle JG, Lanson NA Jr, Smith RB, Casci I, Maltare A, Monaghan J, Nichols CD, Kryndushkin D, Shewmaker F, Pandey UB (2013) RNA-binding ability of FUS regulates neurodegeneration, cytoplasmic mislocalization and incorporation into stress granules associated with FUS carrying ALS-linked mutations. Hum Mol Genet 22:1193–1205.

DeJesus-Hernandez M, et al. (2011) Expanded GGGGCC hexanucleotide repeat in noncoding region of C9ORF72 causes chromosome 9p-linked FTD and ALS. Neuron 72:245–256.

Deniz AA (2020) Networking and dynamic switches in biological condensates. Cell 181:228–230.

Donnelly CJ, Zhang PW, Pham JT, Haeusler AR, Mistry NA, Vidensky S, Daley EL, Poth EM, Hoover B, Fines DM, Maragakis N, Tienari PJ, Petrucelli L, Traynor BJ, Wang J, Rigo F, Bennett CF, Blackshaw S, Sattler R, Rothstein JD (2013) RNA toxicity from the ALS/FTD C9ORF72 expansion is mitigated by antisense intervention. Neuron 80:415–428.

Figley MD, Bieri G, Kolaitis RM, Taylor JP, Gitler AD (2014) Profilin 1 associates with stress granules and ALS-linked mutations alter stress granule dynamics. J Neurosci 34:8083–8097.

Gendron TF, Bieniek KF, Zhang YJ, Jansen-West K, Ash PE, Caulfield T, Daughrity L, Dunmore JH, Castanedes-Casey M, Chew J, Cosio DM, Van BM, Lee WC, Rademakers R, Boylan KB, Dickson DW, Petrucelli L (2013) Antisense transcripts of the expanded C9ORF72 hexanucleotide repeat form nuclear RNA foci and undergo repeat-associated non-ATG translation in c9FTD/ALS. Acta Neuropathol 126:829–844.

Gilks N, Kedersha N, Ayodele M, Shen L, Stoecklin G, Dember LM, Anderson P (2004) Stress granule assembly is mediated by prion-like aggregation of TIA-1. Mol Biol Cell 15:5383–5398.

Guillen-Boixet J, et al. (2020) RNA-induced conformational switching and clustering of G3BP drive stress granule assembly by condensation. Cell 181:346–361.e17.

Haeusler AR, Donnelly CJ, Periz G, Simko EA, Shaw PG, Kim MS, Maragakis NJ, Troncoso JC, Pandey A, Sattler R, Rothstein JD, Wang J (2014) C9orf72 nucleotide repeat structures initiate molecular cascades of disease. Nature 507:195–200.

Jain S, Wheeler JR, Walters RW, Agrawal A, Barsic A, Parker R (2016) ATPase-modulated stress granules contain a diverse proteome and substructure. Cell 164:487–498.

Kedersha N, Tisdale S, Hickman T, Anderson P (2008) Real-time and quantitative imaging of mammalian stress granules and processing bodies. Methods Enzymol 448:521–552.

Kedersha N, Panas MD, Achorn CA, Lyons S, Tisdale S, Hickman T, Thomas M, Lieberman J, McInerney GM, Ivanov P, Anderson P (2016) G3BP-Caprin1-USP10 complexes mediate stress granule condensation and associate with 40S subunits. J Cell Biol 212:845–860.

Kikuchi H, Almer G, Yamashita S, Guegan C, Nagai M, Xu Z, Sosunov A, McKhann GM 2nd, Przedborski S (2006) Spinal cord endoplasmic reticulum stress associated with a microsomal accumulation of mutant superoxide dismutase-1 in an ALS model. Proc Natl Acad Sci USA 103:6025–6030.

Kim EK, Choi EJ (2010) Pathological roles of MAPK signaling pathways in human diseases. Biochim Biophys Acta 1802:396–405.

Kwon I, Xiang S, Kato M, Wu L, Theodoropoulos P, Wang T, Kim J, Yun J, Xie Y, McKnight SL (2014) Poly-dipeptides encoded by the C9orf72 repeats bind nucleoli, impede RNA biogenesis, and kill cells. Science 345:1139–1145.

Lee KH, Zhang P, Kim HJ, Mitrea DM, Sarkar M, Freibaum BD, Cika J, Coughlin M, Messing J, Molliex A, Maxwell BA, Kim NC, Temirov J, Moore J, Kolaitis RM, Shaw TI, Bai B, Peng J, Kriwacki RW, Taylor JP (2016) C9orf72 dipeptide repeats impair the assembly, dynamics, and function of membrane-less organelles. Cell 167:774–788.e17.

Lee S, Shang Y, Redmond SA, Urisman A, Tang AA, Li KH, Burlingame AL, Pak RA, Jovicic A, Gitler AD, Wang J, Gray NS, Seeley WW, Siddique T, Bigio EH, Lee VM, Trojanowski JQ, Chan Jr, Huang EJ (2016) Activation of HIPK2 promotes ER stress-mediated neurodegeneration in amyotrophic lateral sclerosis. Neuron 91:41–55.

Li YR, King OD, Shorter J, Gitler AD (2013) Stress granules as crucibles of ALS pathogenesis. J Cell Biol 201:361–372.

Lin Y, Protter DS, Rosen MK, Parker R (2015) Formation and maturation of phase-separated liquid droplets by RNA-binding proteins. Mol Cell 60:208–219.

Lin Y, Mori E, Kato M, Xiang S, Wu L, Kwon I, McKnight SL (2016) Toxic PR poly-dipeptides encoded by the C9orf72 repeat expansion target LC domain polymers. Cell 167:789–802.e12.

Ling SC, Polymenidou M, Cleveland DW (2013) Converging mechanisms in ALS and FTD: disrupted RNA and protein homeostasis. Neuron 79:416–438.

Liu FL, Morderer D, Wren MC, Vettleson-Trutza SA, Wang YZ, Rabichow BE, Salemi MR, Phinney BS, Oskarsson B, Dickson DW, Rossoll W (2022) Proximity proteomics of C9orf72 dipeptide repeat proteins identifies molecular chaperones as modifiers of poly-GA aggregation. Acta Neuropathol Commun 10:22.

Liu L, Zhang K, Sandoval H, Yamamoto S, Jaiswal M, Sanz E, Li Z, Hui J, Graham BH, Quintana A, Bellen HJ (2015) Glial lipid droplets and ROS induced by mitochondrial defects promote neurodegeneration. Cell 160:177–190.

Medinas DB, Rozas P, Martinez Traub F, Woehlbier U, Brown RH, Bosco DA, Hetz C (2018) Endoplasmic reticulum stress leads to accumulation of wild-type SOD1 aggregates associated with sporadic amyotrophic lateral sclerosis. Proc Natl Acad Sci USA 115:8209–8214.

Mizielinska S, Grönke S, Niccoli T, Ridler CE, Clayton EL, Devoy A, Moens T, Norona FE, Woollacott IO, Pietrzyk J, Cleverley K, Nicoll AJ, Pickering-Brown S, Dols J, Cabecinha M, Hendrich O, Fratta P, Fisher EM, Partridge L, Isaacs AM (2014) C9orf72 repeat expansions cause neurodegeneration in *Drosophila* through arginine-rich proteins. Science 345:1192–1194.

Mori K, Arzberger T, Grasser FA, Gijselinck I, May S, Rentzsch K, Weng SM, Schludi MH, Van Der Zee J, Cruts M, Van BC, Kremmer E, Kretzschmar HA, Haass C, Edbauer D (2013a) Bidirectional transcripts of the expanded C9orf72 hexanucleotide repeat are translated into aggregating dipeptide repeat proteins. Acta Neuropathol 126:881–893.

Mori K, Weng SM, Arzberger T, May S, Rentzsch K, Kremmer E, Schmid B, Kretzschmar HA, Cruts M, Van BC, Haass C, Edbauer D (2013b) The C9orf72 GGGGCC repeat is translated into aggregating dipeptide-repeat proteins in FTLD/ALS. Science 339:1335–1338.

Nishitoh H, Kadowaki H, Nagai A, Maruyama T, Yokota T, Fukutomi H, Noguchi T, Matsuzawa A, Takeda K, Ichijo H (2008) ALS-linked mutant SOD1 induces ER stress- and ASK1-dependent motor neuron death by targeting Derlin-1. Genes Dev 22:1451–1464.

Nishitoh H, Matsuzawa A, Tobiume K, Saegusa K, Takeda K, Inoue K, Hori S, Kakizuka A, Ichijo H (2002) ASK1 is essential for endoplasmic reticulum stress-induced neuronal cell death triggered by expanded polyglutamine repeats. Genes Dev 16:1345–1355.

Ohn T, Kedersha N, Hickman T, Tisdale S, Anderson P (2008) A functional RNAi screen links O-GlcNAc modification of ribosomal proteins to stress granule and processing body assembly. Nat Cell Biol 10:1224–1231.

Protter DS, Parker R (2016) Principles and properties of stress granules. Trends Cell Biol 26:668–679.

Renton AE, et al., ITALSGEN Consortium (2011) A hexanucleotide repeat expansion in C9ORF72 is the cause of chromosome 9p21-linked ALS-FTD. Neuron 72:257–268.

Ritson GP, Custer SK, Freibaum BD, Guinto JB, Geffel D, Moore J, Tang W, Winton MJ, Neumann M, Trojanowski JQ, Lee VM, Forman MS, Taylor JP (2010) TDP-43 mediates degeneration in a novel *Drosophila* model of disease caused by mutations in VCP/p97. J Neurosci 30:7729–7739.

Rossetto D, Avvakumov N, Cote J (2012) Histone phosphorylation: a chromatin modification involved in diverse nuclear events. Epigenetics 7:1098–1108.

Sahana TG, Zhang K (2021) Mitogen-activated protein kinase pathway in amyotrophic lateral sclerosis. Biomedicines 9:969.

Sakae N, Bieniek KF, Zhang YJ, Ross K, Gendron TF, Murray ME, Rademakers R, Petrucelli L, Dickson DW (2018) Poly-GR dipeptide repeat polymers correlate with neurodegeneration and clinicopathological subtypes in C9ORF72-related brain disease. Acta Neuropathol Commun 6:63.

Sanders DW, Kedersha N, Lee DS, Strom AR, Drake V, Riback JA, Bracha D, Eeftens JM, Iwanicki A, Wang A, Wei MT, Whitney G, Lyons SM, Anderson P, Jacobs WM, Ivanov P, Brangwynne CP (2020) Competing protein-RNA interaction networks control multiphase intracellular organization. Cell 181:306–324.e28.

Shi Y, et al. (2018) Haploinsufficiency leads to neurodegeneration in C9ORF72 ALS/FTD human induced motor neurons. Nat Med 24:313–325.

Stricker SH, Koferle A, Beck S (2017) From profiles to function in epigenomics. Nat Rev Genet 18:51–66.

Thams S, Lowry ER, Larraufie MH, Spiller KJ, Li H, Williams DJ, Hoang P, Jiang E, Williams LA, Sandoe J, Eggan K, Lieberam I, Kanning KC, Stockwell BR, Henderson CE, Wichterle H (2019) A stem cell-based screening platform identifies compounds that desensitize motor neurons to endoplasmic reticulum stress. Mol Ther 27:87–101.

Tiwari VK, Stadler MB, Wirbelauer C, Paro R, Schubeler D, Beisel C (2011) A chromatin-modifying function of JNK during stem cell differentiation. Nat Genet 44:94–100.

Urano F, Wang X, Bertolotti A, Zhang Y, Chung P, Harding HP, Ron D (2000) Coupling of stress in the ER to activation of JNK protein kinases by transmembrane protein kinase IRE1. Science 287:664–666.

Walter P, Ron D (2011) The unfolded protein response: from stress pathway to homeostatic regulation. Science 334:1081–1086.

Xu Z, Poidevin M, Li X, Li Y, Shu L, Nelson DL, Li H, Hales CM, Gearing M, Wingo TS, Jin P (2013) Expanded GGGGCC repeat RNA associated with amyotrophic lateral sclerosis and frontotemporal dementia causes neurodegeneration. Proc Natl Acad Sci USA 110:7778–7783.

Yang J, Wu Z, Renier N, Simon DJ, Uryu K, Park DS, Greer PA, Tournier C, Davis RJ, Tessier-Lavigne M (2015) Pathological axonal death through a MAPK cascade that triggers a local energy deficit. Cell 160:161–176.

Yang P, Mathieu C, Kolaitis RM, Zhang P, Messing J, Yurtsever U, Yang Z, Wu J, Li Y, Pan Q, Yu J, Martin EW, Mittag T, Kim HJ, Taylor JP (2020)

G3BP1 is a tunable switch that triggers phase separation to assemble stress granules. Cell 181:325–345.e28.

Zhang K, et al. (2015) The C9orf72 repeat expansion disrupts nucleocytoplasmic transport. Nature 525:56–61.

Zhang K, Daigle JG, Cunningham KM, Coyne AN, Ruan K, Grima JC, Bowen KE, Wadhwa H, Yang P, Rigo F, Taylor JP, Gitler AD, Rothstein JD, Lloyd TE (2018) Stress granule assembly disrupts nucleocytoplasmic transport. Cell 173:958–971.e17.

Zhang YJ, et al. (2014) Aggregation-prone c9FTD/ALS poly(GA) RAN-translated proteins cause neurotoxicity by inducing ER stress. Acta Neuropathol 128:505–524.

Zhang YJ, et al. (2018) Poly(GR) impairs protein translation and stress granule dynamics in C9orf72-associated frontotemporal dementia and amyotrophic lateral sclerosis. Nat Med 24:1136–1142.

Zhang YJ, et al. (2019) Heterochromatin anomalies and double-stranded RNA accumulation underlie C9orf72 poly(PR) toxicity. Science 363: eaav2606.

Zu T, Liu Y, Banez-Coronel M, Reid T, Pletnikova O, Lewis J, Miller TM, Harms MB, Falchook AE, Subramony SH, Ostrow LW, Rothstein JD, Troncoso JC, Ranum LP (2013) RAN proteins and RNA foci from antisense transcripts in C9ORF72 ALS and frontotemporal dementia. Proc Natl Acad Sci USA 110:E4968–E4977.